I

Randelhoff, A. and J. D. Guthrie (2016), Regional patterns in current and future export production in the central Arctic Ocean quantified from nitrate fluxes, *Geophysical Research Letters*, *43*, 8600–8608, doi:10.1002/2016gl070252.

AGU PUBLICATIONS

Geophysical Research Letters

RESEARCH LETTER
10.1002/2016GL070252

Key Points:
- Vertical nitrate flux contributes significantly to current CAO export production
- Regional differences in turbulent mixing and stratification lead to varying responses of primary production to climate change across the CAO
- Future increases in Atlantic sector EP possibly offset by reduced nitrate fluxes in other CAO regions

Correspondence to:
A. Randelhoff,
achim@npolar.no

Citation:
Randelhoff, A., and J. D. Guthrie (2016), Regional patterns in current and future export production in the central Arctic Ocean quantified from nitrate fluxes, *Geophys. Res. Lett., 43*, 8600–8608, doi:10.1002/2016GL070252.

Received 30 JUN 2016
Accepted 3 AUG 2016
Accepted article online 5 AUG 2016
Published online 24 AUG 2016

Regional patterns in current and future export production in the central Arctic Ocean quantified from nitrate fluxes

Achim Randelhoff[1,2] and John D. Guthrie[3]

[1]Institute for Arctic and Marine Biology, University of Tromsø, Tromsø, Norway, [2]Norwegian Polar Institute, Tromsø, Norway, [3]Polar Science Center, Applied Physics Lab, University of Washington, Seattle, Washington, USA

Abstract Due to severe nutrient and light limitation, the central Arctic Ocean has been characterized as a region of low primary productivity, with high retention of carbon in the surface waters. Using an in-depth analysis of published and new measurements of turbulent microstructure and high-resolution profiles of nitrate concentration, we reassess the vertical supply of nitrate to the Polar Mixed Layer and the associated export of particulate organic matter across the nitracline. We estimate annual export production to be approximately 1.5–3 g C m^{-2}, but regional differences in both current and future potential of export production are large, with the eastern Arctic being least constrained by vertical nutrient supply and the western Arctic the most. Future changes in export production are assessed using a 1-D budget model; increases in the Atlantic sector are possibly compensated by decreases in the rest of the central Arctic Ocean such that the net change might be insignificant.

1. Introduction

The central Arctic Ocean (CAO) is strongly stratified in the surface, which limits nutrient supply to the photic zone and constrains Arctic Ocean primary production [e.g., *Tremblay et al.*, 2015]. Various halocline structures are present throughout the CAO, but a common feature is their perennial persistence as opposed to on the shelves, where relatively strong mixing can homogenize vertical stratification during the winter [e.g., *Aagaard and Carmack*, 1994; *Randelhoff et al.*, 2015]. The halocline separates the Polar Mixed Layer (PML), where primary production takes place, from Atlantic (AW) or Pacific Water (PW) at intermediate depths. Due to the dependence of primary production on sunlight, upper ocean nutrient concentrations vary strongly with season, and a part of its nitrogen pool is exported across the pycnocline as biogenic particulate organic nitrogen.

PW and AW are the main sources of nutrients in the Arctic Ocean [*Torres-Valdés et al.*, 2013], driving the replenishment of the PML nutrient inventory from below, thus ensuring a steady seasonal cycle of nutrient concentrations in the surface waters.

Previous findings indicate fairly low productivity in the deep basins of the Arctic Ocean, between 10 and several tens of g C m^{-2} yr^{-1} based on various methods like oxygen concentration [*Pomeroy*, 1997; *Zheng et al.*, 1997], incubations [*Cota et al.*, 1996; *Gosselin et al.*, 1997] and annual drawdown of nutrients [*Codispoti et al.*, 2013]. The export flux has been estimated to be even lower at less than 1 g C m^{-2} yr^{-1} [*Anderson et al.*, 2003; *Cai et al.*, 2010; *Honjo et al.*, 2010], and *Olli et al.* [2007] attributed low export estimates to high grazing pressure of zooplankton expatriates advected from the shelves. Thus, the picture of CAO nutrient cycling that has emerged is one of low export efficiency driven by intense recycling of organic matter in the shallow photic zone, with very little potential for carbon sequestration [*Wassmann et al.*, 2004]. However, in studies of CAO productivity and nutrient cycling, the role of vertical mixing is usually treated only qualitatively, where the strong stratification is invoked to infer weak vertical fluxes without further differentiation.

Measuring the turbulent vertical flux of nitrate across the perennial nitracline of the Arctic Ocean takes advantage of two features: Its persistence ensures little seasonality in the flux magnitude compared to the seasonal nitracline that may appear in the summer months in the Eastern Arctic, and second, it is sufficiently removed from the ocean surface such that turbulent mixing intensities are not dictated by intermittent atmospheric, shear-driven mixing. To balance the budget, the upward vertical flux of nitrate (NO_3^-) is an estimate of the downward vertical flux of particulate organic nitrogen minus what is supplied by horizontal advection. Due to large residence times, the horizontal ventilation of the CAO surface waters contributes only a small amount

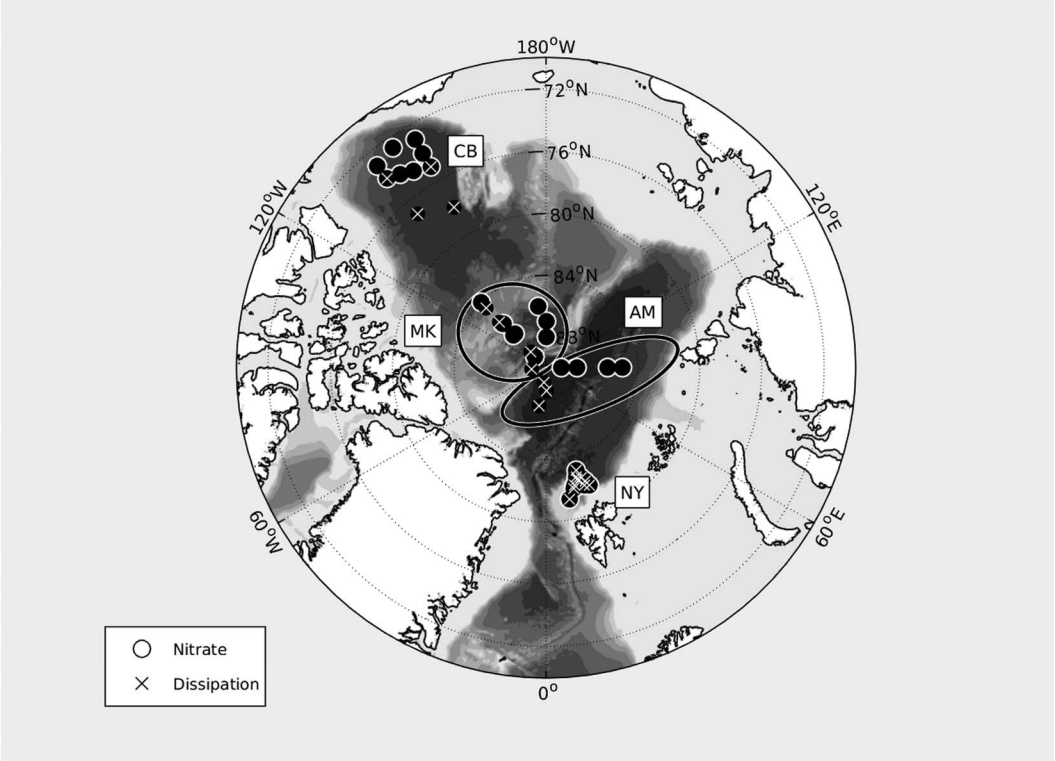

Figure 1. Map of sample locations, indicating the four regions: Nansen Basin/Yermak Plateau (NY), Amundsen Basin (AM), Makarov Basin (MK), and Canada Basin (CB).

of nutrients to the PML, amounting to approximately 0.5 g C m^{-2} yr^{-1} [*Anderson et al.*, 2003]. Therefore, the vertical supply of nitrate also places a bound on NO_3^--based production in the PML.

In this study, we set out to quantify regional patterns in the current export production that is supported by the vertical (and horizontal) resupply of nitrate and assess what future export production might be like given climate-related trends in the freshwater budget, sea ice cover, and turbulent mixing.

2. Methods

2.1. Data

This study combines new observations in the Nansen Basin/Yermak Plateau region with a reanalysis of similar, previously published data from other parts of the CAO.

Colocated continuous vertical profiles of (sensor-based) nitrate concentrations ($\mathcal{N}$) and turbulent microstructure were collected during the January–June 2015 N-ICE ice camp in the Nansen Basin and in the vicinity of the Yermak Plateau north of Svalbard (Figure 1; see *Granskog et al.* [2016] for details). All of the N-ICE profiles included in this study were located at water depths >1500 m.

Vertical profiles of conductivity, temperature, and depth (CTD) and nitrate concentration data in the Amundsen, Makarov, and Canada Basins obtained through the North Pole Environmental Observatory (NPEO) in 2007 and 2008 [*Alkire et al.*, 2010] have been downloaded from https://arcticdata.io/catalog/#view/doi:10.18739/A2HK6Z and https://arcticdata.io/catalog/#view/doi:10.18739/A2WS4P.

Microstructure profiles collected in the Amundsen Basin close to the North Pole (provided by Ilker Fer) were analyzed for dissipation in the nitracline. These microstructure measurements are published and described in more detail by *Fer* [2009], *Sirevaag and Fer* [2012], and *Guthrie et al.* [2013].

The Makarov Basin dissipation estimate is derived from a subset of eXpendable current profiler (XCP) and CTD profiles collected as part of NPEO in 2007. The Canada Basin dissipation estimate is derived from 3 years of current meter data from four moorings deployed as part of the Beaufort Gyre Exploration Project (BGEP).

We group the data into four geographical regions: NY (Nansen Basin/Yermak Plateau), AM (Amundsen Basin), MK (Makarov Basin), and CB (Canada Basin) (see Figure 1). The distinction drawn here between the hydrografies of the Makarov and Amundsen Basins might change on decadal timescales, depending on the atmospheric forcing of freshwater budgets and the Transpolar Drift [e.g., *Morison et al.*, 2012], but for the 2007/2008 NPEO data, the location of the Lomonosov Ridge is a natural separation between the two regimes.

2.2. Dissipation Estimates

Microstructure data, collected using a MSS90-L profiler (IWS Wassermesstechnik, Germany), were processed following *Fer* [2006]. Assuming local small-scale isotropy [*Yamazaki and Osborn*, 1990], dissipation of turbulent kinetic energy was estimated from the measured microscale shear as $\epsilon = 7.5\nu\langle\left(\partial_z u'\right)^2\rangle$, where ν is the molecular viscosity of sea water and $\partial_z u'$ the turbulent shear. The processing is similar across all the microstructure data sets used in this study.

The dissipation estimates for the Makarov and Canada Basins are derived from a widely validated fine-scale parameterization based on 10 m shear variance relative to Garrett-Munk values [*Garrett and Munk*, 1975]. For full details of the parameterization, see *Kunze et al.* [2006]. The processing and analysis is described in more detail by *Guthrie et al.* [2013]. The calculation of the BGEP dissipation values is described fully by *Lique et al.* [2014]. *Guthrie et al.* [2013] showed excellent agreement between dissipation estimates derived from MSS microstructure observations and this finescale parameterization.

2.3. CTD and Nitrate Concentration Data

Processing of nitrate concentration profiles, measured using an ISUS sonde (Satlantic; V3 during N-ICE and V2 for the NPEO data), made use of the "temperature compensated, salinity subtracted" algorithm of *Sakamoto et al.* [2009], using a waveband of 217–240 nm. Although final nitrate concentrations measured by the ISUS can have uncertainties of up to 1 μM, this is mostly due to a depth-independent bias, such that vertical gradients are resolved accurately [*Randelhoff et al.*, 2016]. The bias was taken care of by calibrating output against bottle samples on all campaigns. Further details of the processing of ISUS data are described, e.g., by *Alkire et al.* [2010] and *Randelhoff et al.* [2016].

2.4. Nitrate Fluxes

In order to calculate the nitrate flux $F_{\mathcal{N}} = -K_\rho \frac{\partial \mathcal{N}}{\partial z}$ across the perennial nitracline, we need to combine profiles of turbulent mixing (vertical eddy diffusivity K_ρ) and nitrate concentrations ($\mathcal{N}$). This requires special care since both $K_\rho = 0.2\frac{\epsilon}{N^2}$ [*Osborn*, 1980], (ϵ being the dissipation) and $\mathcal{N}$ gradients depend on the vertical density stratification (buoyancy frequency $N^2 = -\frac{g}{\rho}\frac{\partial \rho}{\partial z}$), which can be different at different times and locations. The above definition of $F_{\mathcal{N}}$ is equivalent to

$$F_{\mathcal{N}} = 0.2\epsilon \frac{\rho}{g}\frac{\partial \mathcal{N}}{\partial \sigma_\theta}, \tag{1}$$

where we first inserted the K_ρ estimation formula and then the definition of N^2. This representation is more convenient for two reasons: First, we can ignore changes in isopycnal heights between profiles. Second, it more accurately reflects the gradients between the different water mass end-members. Otherwise, if we used K_ρ instead, we would have to adjust it for the actual buoyancy frequency in every nitrate profile.

Close to the inflow of Atlantic Water (Nansen Basin/Yermak Plateau), the $\frac{\partial \mathcal{N}}{\partial \sigma_\theta}$ slope is depth independent for each profile, while the additional end-members (PML, upper and lower halocline waters and AW) lead to variable slopes in the Canada and Makarov Basins (Figure 2a). The following criteria captured the regional patterns in nitracline distribution: For the Nansen/Yermak and Amundsen Basin, $\frac{\partial \mathcal{N}}{\partial \sigma_\theta}$ was calculated across the interval 50 to 90 m. For the Makarov Basin, $\frac{\partial \mathcal{N}}{\partial \sigma_\theta}$ was calculated over the interval from salinity $S = 32$ down to either 80 m depth or $S = 32.5$, whichever was deeper. For the Canada Basin, the slope was calculated over the σ_θ range from 25 to 26 kg m^{-3}. All individual regressions were checked visually.

To convert $F_{\mathcal{N}}$ to equivalent units of g C m^{-2} yr^{-1}, we employ a constant C:N Redfield ratio of 106:16. Any errors made by this assumption are linear and thus easily controlled.

2.5. A Simple 1-D Model for the Polar Mixed Layer Nitrate Budget

We can take advantage of the perennial nitrate gradient merely as a diagnostic tool to estimate year-round nitrate fluxes (and indirectly, export production), not attributing any role of the turbulent mixing in forcing or limiting upper ocean primary productivity. Concretely, if the productivity was increased or the vertical diffusivity decreased, the nitrate gradient would steepen in order to make $F_{\mathcal{N}}$ match the surface drawdown.

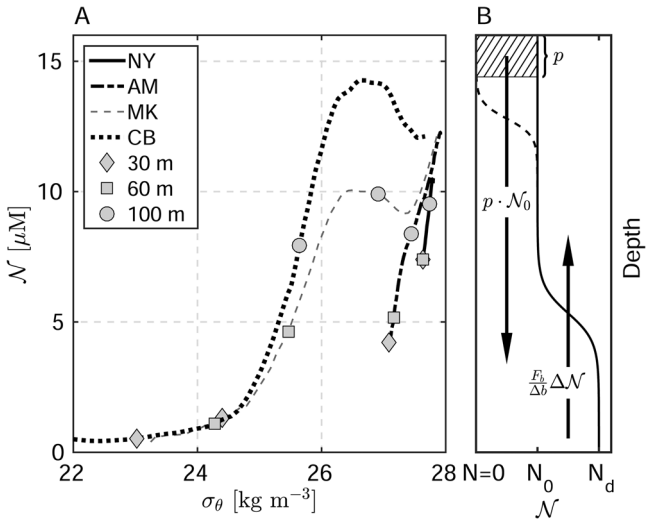

Figure 2. Vertical stratification of density and nitrate in the CAO. (a) $\mathcal{N}$-σ_θ profiles averaged by region (see Figure 1). Diamonds, squares, and circles indicate different depths. (b) Conceptual model of vertical $\mathcal{N}$ profiles with associated vertical nitrogen fluxes (see text). The seasonal nitracline (dashed line) is decoupled from the perennial nitracline. A layer of thickness p [year] (hatched area) corresponds to that fraction $p \cdot \mathcal{N}_0$ of the seasonal nitrate drawdown that is exported below the perennial nitracline, while the rest might be remineralized before reaching deep enough. Across the perennial nitracline, the vertical nitrate flux is $F_\mathcal{N} = \frac{F_b}{\Delta b}\Delta\mathcal{N} \equiv \frac{F_b}{\Delta b}(\mathcal{N}_d - \mathcal{N}_0)$.

However, since this also leads to a lower surface $\mathcal{N}$ and accordingly annual nitrate drawdown is decreased, the result is best described as the steady state of a system of coupled equations. In fact, the decomposition of $F_\mathcal{N}$ into the product of ϵ and $\frac{\partial\mathcal{N}}{\partial\sigma_\theta}$ provides a different perspective by condensing the vertical gradients into one quantity $\frac{\partial\mathcal{N}}{\partial\sigma_\theta}$ only related to $\mathcal{N}$ and σ_θ in the end-members that mix across the nitracline.

Assuming annual new production is proportional to the prebloom surface nitrate pool, export production (EP) can be described as EP $= p \cdot \mathcal{N}_0$ with the surface nitrate concentration $\mathcal{N}_0$ and a hypothetical "nitrate drawdown velocity scale" p. The parameter p is at most equal to but likely smaller than the depth of seasonal nitrate depletion (divided by [1 year]), which depends on photic zone depth, seasonal surface layer stratification, and possibly community structure; this is because we can expect that some of the consumed nitrogen is remineralized before reaching below the perennial nitracline (Figure 2b). The export production has to match the sum of the upward turbulent diffusive flux and other terms (like horizontal advection of nitrate and convective entrainment during winter); the sum of the latter is denoted by A in the following. Rewriting $\frac{\partial\mathcal{N}}{\partial\sigma_\theta}$ from equation (1) as a straight mixing line between the end-members above and below the nitracline (Figure 2a), the vertical flux becomes $F_\mathcal{N} = 0.2\epsilon\frac{\rho}{g}\frac{\mathcal{N}_d - \mathcal{N}_0}{\rho_d - \rho_0}$, where indices d and 0 refer to deep (below nitracline) and above nitracline end-members, respectively. Equating EP and $F_\mathcal{N} + A$ yields

$$\mathrm{EP} = p\frac{\frac{F_b}{\Delta b}\mathcal{N}_d + A}{p + \frac{F_b}{\Delta b}}, \tag{2}$$

where $F_b = 0.2\epsilon$ is the buoyancy flux and $\Delta b = g\frac{\rho_d - \rho_0}{\rho}$ the buoyancy difference between above and below nitracline. The ratio of the two yields a mass flux velocity scale representing the integrated effect of turbulent mixing and perennial stratification. The "drawdown velocity scale" p integrates mainly the effects of photic zone depth and seasonal stratification. Equation (2) shows that at large values of either $\frac{F_b}{\Delta b}$ or p, the other becomes limiting. For example, for high p, that is, when light is not limiting and seasonal mixing makes all nitrate in the PML accessible to primary producers, the maximum nitrate flux is

$$F_{\mathcal{N},\max} = \frac{F_b}{\Delta b}\mathcal{N}_d. \tag{3}$$

For each region, p and $\frac{F_b}{\Delta b}$ are estimated using average values of surface $\mathcal{N}_0$ and buoyancy difference Δb across the nitracline derived from each profile in that region (see Table 1, cf. also Figure 2). The parameter

Table 1. Mean Values of Key Parameters Grouped by Region (See Figure 1)[a]

Region	$F_{\mathcal{N}}$ (g C m^{-2} yr^{-1})	$\frac{\partial \mathcal{N}}{\partial \sigma_\theta}$ (mmol kg^{-1})	ϵ (W kg^{-1})	p (m yr^{-1})	$F_b/\Delta b$ (m yr^{-1})	$F_{\mathcal{N},\max}$ (g C m^{-2} yr^{-1})	$F_{\mathcal{N},\max(2100)}$ (g C m^{-2} yr^{-1})
NY	7.0	20 ± 5 [$n = 10$]	$6.0\ (3.5, 12) \cdot 10^{-9}$ [$n = 37$]	13	30	24	12
AM	1.8	14 ± 1 [$n = 6$]	$2.6\ (1.6, 4.2) \cdot 10^{-9}$ [$n \approx 600$]	7	4	3.2	1.6
MK	0.5	7 ± 0.3 [$n = 9$]	$1.5\ (0.9, 2.8) \cdot 10^{-9}$ [$n = 4$]	11	0.6	0.5	0.3
CB	0.4	10 ± 0.1 [$n = 8$]	$0.7\ (0.5, 1.0) \cdot 10^{-9}$[b]	21	0.5	0.4	0.4

[a]NY: Nansen Basin/Yermak Plateau, AM: Amundsen Basin, MK: Makarov Basin, CB: Canada Basin. $F_{\mathcal{N}}$: Vertical diffusive nitrate flux through the nitracline converted to equivalent carbon units (see text; for a discussion regarding convective entrainment, see section 4.1); $F_{\mathcal{N},\max}$: maximum nitrate flux currently possible; $F_{\mathcal{N},\max(2100)}$: possible value for maximum nitrate flux by 2100 in an RCP8.5 scenario (see text); mean $\frac{\partial \mathcal{N}}{\partial \sigma_\theta}$ (evaluated across the nitracline of every individual profile, $\pm$ standard deviation between profiles); ϵ: mean nitracline dissipation rate (in parentheses: 95% confidence intervals); p: nitrate drawdown velocity scale; $F_b/\Delta b$: buoyancy flux divided by buoyancy difference across nitracline (see text). In square brackets: number of profiles (n).

[b]Four moorings over 3 years (see text).

p is calculated as $p \equiv \mathrm{EP}/\mathcal{N}_0^*$, where we estimate EP as the sum of $F_{\mathcal{N}}$ and horizontal advection (roughly 0.5 g C m^{-2} yr^{-1}, see *Anderson et al.* [2003]). $\frac{F_b}{\Delta b}$ is based on the buoyancy difference between just above the nitracline and the level where $\mathcal{N}_d^* = 10$ µM. However, note that the exact choice of $\mathcal{N}_d^*$ is not crucial as long as it is inside the range where $\frac{\partial \mathcal{N}}{\partial \sigma_\theta}$ is constant and we evaluate Δb relative to the same depth.

3. Results

The four different regions showed considerable differences, where σ_θ-$\mathcal{N}$ slopes, dissipation rates, and accordingly $F_{\mathcal{N}}$ were largest in the east (Nansen Basin/Yermak and Amundsen Basin) and smallest in the west (Makarov and Canada Basins) (see Figure 1, Table 1). Overall, $F_{\mathcal{N}}$ ranged between 0.4 and 7 g C m^{-2} yr^{-1}. The p values are located in a relatively narrow range between 7 and 21 m yr^{-1} for all profiles, while $\frac{F_b}{\Delta b}$ varies strongly between 0.5 and 30 m yr^{-1}.

The maximum $F_{\mathcal{N},\max}$ the mixing can support (following equation (3)) is equal to present-day $F_{\mathcal{N}}$ in the Canadian Basin, only slightly larger in the Amundsen Basin (3.2 g C m^{-2} yr^{-1}) and largest in the Yermak Plateau region of the Nansen Basin (24 g C m^{-2} yr^{-1}) (Table 1). Since Amundsen Basin p would have to increase by several tens of m yr^{-1} in order to achieve this increase, we can consider the Amundsen Basin to be practically nutrient-limited, but not as strictly as the Canada and Makarov Basins. Nansen Basin/Yermak Plateau region EP, however, is not limited by nutrients.

4. Discussion

4.1. Stratification and Mixing

As expected, turbulent mixing is much stronger in the relative vicinity of the Yermak Plateau than in the otherwise extremely quiescent CAO. In addition, the low PML salinities in the western Arctic lead to smaller σ_θ-$\mathcal{N}$ slopes than in the East and thus very small $F_{\mathcal{N}}$. However, it is not primarily the stratification, but the low mixing levels that suppress vertical fluxes of nitrate in the Canadian Arctic. Since upper ocean stratification also enhances the under-ice dissipation mechanism outlined by *Morison et al.* [1985], it could be responsible for removing energy from the internal wave field such that less small-scale mixing can penetrate into the nitracline [*Guthrie et al.*, 2013]. Since the double-diffusive staircases are located much deeper (starting from around 200 m [*Timmermans et al.*, 2008]) than the nitracline, double-diffusive convection is not a mode for vertical transport of nitrate.

The "true" $F_{\mathcal{N}}$ values are probably slightly higher than the estimates presented here for two reasons: First, the NPEO data used in this study were all sampled in early spring, just before the onset of melting or primary production. Vertical nitrate gradients are therefore at their weakest, reducing the flux somewhat. However, seeing that NO_3^- inventories in the Canada and Makarov Basins are extremely low to begin with, this effect is probably not significant, and might be more important in the eastern Arctic data. Second, also the Makarov and Amundsen Basin fine/microstructure data was sampled in early spring. *Dosser and Rainville* [2016] find

that internal wave amplitudes are 16% higher during the summer when low ice concentrations facilitate input of near-inertial energy, which indicates somewhat but not much higher $F_{\mathcal{N}^*}$ values than we calculated for this study.

In addition, (haline) winter convection can entrain a certain portion of the nitracline into the Polar Mixed Layer. Because average buoyancy fluxes (estimated as 0.2ϵ) across the pycnocline can only balance at most a few percent of the seasonal sea ice meltwater input, we can use the seasonal accumulation of meltwater as an estimate for winter convection. The findings of *McPhee et al.* [1998] and *Timmermans et al.* [2011] thus indicate a convection-derived density surplus of approximately 20 kg m^{-2}. To estimate regional patterns and the orders of magnitude of nitrate entrainment by convection, we assume that about half of this buoyancy flux goes into erasing the seasonal stratification and the other half could potentially entrain nitrate from the upper nitracline. The entrainment flux can be estimated by distributing this density surplus, keeping the mixed layer unstratified, and integrating the additional nitrate down to the convection depth. The western Arctic is strongly salinity stratified even above the nitracline (Figure 2) such that this convection cannot penetrate very deep into the nitracline. Accordingly, we estimate an additional $F_{\mathcal{N}^*,\text{convective}} = 0.01$ and 0.05 g C m^{-2} yr^{-1} for the Canada and Makarov Basins, respectively. However, the low-$\mathcal{N}^*$ surface layer is unstratified in our data from the Eastern Arctic, so our method yields considerably higher estimates of $F_{\mathcal{N}^*,\text{convective}} = 1$ and 2 g C m^{-2} yr^{-1} for the Amundsen Basin and the Nansen Basin/Yermak Plateau data, respectively, but it must be stressed that these numbers are mostly indicative of regional trends and the absolute magnitudes are likely smaller since wind mixing rarely reaches deep enough that it could help with entraining heavier water into the deep mixed layers of the Eurasian Basin.

4.2. Arctic Ocean Productivity

Weighting the individual $F_{\mathcal{N}^*}$ estimates by the areas of the basins they cover (the Nansen/Yermak estimate is extended across the western Nansen Basin and along the shelf slope, covering $2 \cdot 10^{11}$ m^2), the average upward nitrate flux across all four regions is 1.5 ± 0.5 g C m^{-2} yr^{-1}, where the uncertainty stems from stipulating an uncertainty of approximately 10% in the area weights. In addition, the convective entrainment of nitrate (assuming it is represented by the numbers as detailed in the previous section) provides another 0.5 g C m^{-2} yr^{-1}. Horizontal advection supplies another 0.5 g C m^{-2} yr^{-1} [*Anderson et al.*, 2003]. In total, this accumulates to an export production somewhere between 1.5 and 3 g C m^{-2} yr^{-1}.

This is significantly higher than the 0.6–1.3 g C m^{-2} yr^{-1} value that *Anderson et al.* [2003] found using phosphate deficits and residence time of the end-members constituting the PML. Although they included some estimates of the diapycnal mixing, all of these represent very weak mixing ($K_\rho = 1–7 \cdot 10^{-6}$ m^2 s^{-1}) at the lower end of observed values. The present study indicates that their analysis somewhat underestimated the importance of the vertical supply of nutrients, although the difference in terms of absolute values of export production is very small.

Cai et al. [2010] estimated the particulate organic carbon flux at 100 m depth over the Central Arctic from Thorium-234 measurements in late summer to be what is equal to 0.9 g C m^{-2} yr^{-1}, consistent with our value when excluding the high flux in the area close to the Yermak Plateau. *Honjo et al.* [2010] measured daily fluxes of particulate organic carbon at 120 and 200 m depth over the deep Beaufort Gyre ranging between what is equal to 0.05 and 0.65 g C m^{-2} yr^{-1}, but the seasonal distribution is not well resolved. These values are smaller than what we infer for the Canada Basin, but comparable considering that the Beaufort Gyre has longer residence times than the rest of the Canada Basin and therefore receives less horizontal nutrient input [*Anderson et al.*, 2003].

Anderson et al. [2003] caution against the use of nitrate as a tracer for assessing export production due to uncertainties surrounding nitrification, denitrification, and nitrogen fixation. We assume that denitrification, requiring low levels of dissolved oxygen, is not an issue when the water has left the shallow shelves. Nitrification does not disturb the nitrogen budget as it simply counts toward regenerated production [e.g., *Tremblay et al.*, 2015]. Nitrogen fixation in the Arctic Ocean is still an open question. For the Canadian Arctic, *Blais et al.* [2012] identify the Mackenzie River as a source of diazotrophs and find nitrogen fixation rates of 0.14 μmol N m^{-3} d^{-1} for the southern Beaufort Sea, which (assuming a seasonal mixed layer depth of 25 m) could contribute at most 0.1 g C m^{-2} in annual production — potentially appreciable, but negligible in the context of all the other uncertainties surrounding our estimates.

Based on nutrient-drawdown-based estimates of net community production (NCP), *Codispoti et al.* [2013] infer that production in the Eurasian Basin is not nutrient limited but rather light limited. However, their winter data are biased toward the vicinity of the Yermak Plateau where nutrient concentrations are higher, which skews NCP estimates. Our findings indicate that NCP in the Amundsen Basin is still nutrient limited and that among our study regions, only Nansen Basin NCP in the vicinity of the Yermak Plateau is not limited by nutrients at all.

Note how the drawdown velocity of around 10 to 20 m yr^{-1} coincides with the scale of the vertical extent of the seasonal meltwater-induced upper ocean stratification in the Arctic summer [see also *McPhee et al.*, 1987; *Randelhoff et al.*, 2014]. This scale is also representative of the depth of nitrate depletion early in the season before the subsurface chlorophyll maximum has consumed a large part of the nutrients below the seasonal pycnocline [*Randelhoff et al.*, 2016]. Although it therefore is an attractive idea to associate blooms with high export efficiencies, the link between primary production during phytoplankton blooms and the associated export of particulate matter remains elusive.

4.3. Future Evolution of Arctic Primary Production

By way of the 1-D mixed-layer $\mathcal{N}$ budget presented above, the implications of the predicted acceleration of the hydrological cycle, accompanying increase of freshwater storage in the surface mixed layer and trends in seasonal ice melt become easier to interpret.

Increasing summer ice melt rates will strengthen seasonal stratification and entail smaller upward nitrate fluxes through the seasonal pycnocline, but if the melt rates are high enough to melt most of the ice before the end of summer, seasonal stratification will weaken again as a result of the reduced freshwater input at the surface, leading to more nitrate assimilation [*Randelhoff et al.*, 2016]. In addition, a less dense ice cover will also permit more input of wind energy, driving nitracline dissipation. An increase in photic zone depth might lead to an increase in p. Because of uncertainties as to how much of the consumed nitrogen is actually exported under changed nutrient loading, the fate of p is unclear, but if anything, it will likely increase.

The (nutrient-poor) freshwater runoff feeding into the Arctic Ocean is predicted to increase significantly [*Bintanja and Selten*, 2014; *Haine et al.*, 2015], strengthening stratification at the base of the PML [*Nummelin et al.*, 2015]. Vertical mixing is a complicated issue with many faces. Even neglecting the speculative changes in nitracline dissipation, it is illustrative to consider the possible impacts of changing stratification alone since its response is relatively robust as the freshwater input to the Arctic increases. To this end, we extracted 21st century projections of CAO stratification from the RCP8.5 run of the Norwegian Earth System model [*Bentsen et al.*, 2013; *Iversen et al.*, 2013]. Comparing the 2005–2015 and the 2090–2100 mean density fields and grouping them into our four subregions, we find that below-PML stratification (expressed as N^2, i.e., $\sim \Delta b$) approximately doubles by the end of the century in all four subregions except for the Canada Basin where it remains unchanged. Changing $F_b/\Delta b$ accordingly and calculating the updated maximum vertical nitrate flux $F_{\mathcal{N},\mathrm{max}(2100)}$, we find that by 2100, there is the distinct potential that the enhanced stratification alone reduces export production in most areas of the CAO (Table 1). While these numbers are only indicative of the relative trends, they suggest that possible increases of export production close to the Atlantic inflow ("NY" region) are offset by decreases in the other regions; even though the CAO-average $F_{\mathcal{N},\mathrm{max}(2100)}$ is slightly higher than the current estimate, the difference is not significant (1.7 g C m^2 yr^{-1} versus 1.4 g C m^2 yr^{-1} before rounding within uncertainty).

5. Summary and Perspectives

In this study, we have formalized and quantified current export production in the CAO. By and large, our study confirms the common argument that CAO export production is mostly constrained by nutrient availability, and our study indicates that it will be even more so in a future, even more stratified CAO. We suggest that CAO export production is between 1.5 and 3 g C m^{-2} yr^{-1}, which is slightly more than previously assumed but still very small.

More importantly, there exist horizontal gradients along a transect crossing the deep basins of the Arctic Ocean from west to east. In the west, the strong haline stratification and low levels of mixing conspire to constrain nutrient availability. In the east, the near-surface inflow of saltier Atlantic Water leads to weak vertical stratification, which together with elevated turbulent mixing close to the Yermak Plateau and the shelf region alleviates nutrient limitation, and instead makes the seasonal stratification and light availability a limiting factor. The problem of predicting future CAO export production has thus been framed in terms of an "upward

flux velocity scale" $\frac{F_b}{\Delta b}$ and a "nutrient drawdown velocity scale" p. Although climate-related changes in the density field alone are sufficient to drive markedly regional changes in nutrient supply to the photic zone, more work is needed to (a) predict the relative magnitude of changes in F_b and Δb, and (b) understand how p is related to seasonal stratification, photic zone depth, and export efficiency as a function of community structure.

Acknowledgments

A.R.'s work was supported through the project CARBON BRIDGE: Bridging marine productivity regimes: How Atlantic advective inflow affects productivity, carbon cycling, and export in a melting Arctic Ocean, a Polar Programme (project 226415) funded by the Norwegian Research Council. J.G. was funded through National Science Foundation projects ARC-0909408 and ARC-0856330. N-ICE data collection was supported by the Norwegian Polar Institute's Centre for Ice, Climate and Ecosystems (ICE) through the N-ICE project, with additional support from the Ministry of Climate and Environment, and Ministry of Foreign Affairs of Norway. We thank the captains and crews of R/V *Lance* and all the scientists involved in the N-ICE field campaign for their support. The Makarov and Amundsen Basin ISUS and the Makarov Basin XCP data were collected through the North Pole Environmental Observatory in 2007 and 2008. The Canada Basin ISUS and MMP mooring data were collected through the Beaufort Gyre Exploration Program. Both projects were funded by the National Science Foundation. Ilker Fer provided the Amundsen Basin dissipation profiles. Aleksi Nummelin assisted with extracting the NorESM model results. We thank Arild Sundfjord for helpful comments on an earlier version of this paper. Two anonymous reviewers helped greatly to clarify the presentation of the material. N-ICE data are available through the Norwegian Polar Data Centre at https://data.npolar.no/dataset/96eb41f9-c620-5fe4-a7a3-96b0e55fd3d5 (ISUS) and https://data.npolar.no/dataset/774bf6ab-b27e-51ab-bf8c-eb866cf61be2 (MSS).

References

Aagaard, K., and E. C. Carmack (1994), The Arctic Ocean and climate: A perspective, in *The Polar Oceans and Their Role in Shaping the Global Environment*, edited by O. M. Johannessen, R. D. Muench, and J. E. Overland, pp. 5–20, AGU, Washington, D. C., doi:10.1029/GM085p0005

Alkire, M. B., K. K. Falkner, J. Morison, R. W. Collier, C. K. Guay, R. A. Desiderio, I. G. Rigor, and M. McPhee (2010), Sensor-based profiles of the NO parameter in the central Arctic and southern Canada Basin: New insights regarding the cold halocline, *Deep Sea Res., Part I*, *57*(11), 1432–1443, doi:10.1016/j.dsr.2010.07.011.

Anderson, L. G., E. P. Jones, and J. H. Swift (2003), Export production in the central Arctic Ocean evaluated from phosphate deficits, *J. Geophys. Res.*, *108*(C6), 3199, doi:10.1029/2001JC001057.

Bentsen, M., et al. (2013), The Norwegian Earth system model, NorESM1-M—Part 1: Description and basic evaluation of the physical climate, *Geosci. Model Dev.*, *6*(3), 687–720, doi:10.5194/gmd-6-687-2013.

Bintanja, R., and F. M. Selten (2014), Future increases in Arctic precipitation linked to local evaporation and sea-ice retreat, *Nature*, *509*(7501), 479–482.

Blais, M., J.-E. Tremblay, A. D. Jungblut, J. Gagnon, J. Martin, M. Thaler, and C. Lovejoy (2012), Nitrogen fixation and identification of potential diazotrophs in the Canadian Arctic, *Global Biogeochem. Cycles*, *26*, GB3022, doi:10.1029/2011GB004096.

Cai, P., M. Rutgers van der Loeff, I. Stimac, E.-M. Nöthig, K. Lepore, and S. B. Moran (2010), Low export flux of particulate organic carbon in the central Arctic Ocean as revealed by ^{234}Th:^{238}U disequilibrium, *J. Geophys. Res.*, *115*, C10037, doi:10.1029/2009JC005595.

Codispoti, L., V. Kelly, A. Thessen, P. Matrai, S. Suttles, V. Hill, M. Steele, and B. Light (2013), Synthesis of primary production in the Arctic Ocean: III. Nitrate and phosphate based estimates of net community production, *Prog. Oceanogr.*, *110*, 126–150, doi:10.1016/j.pocean.2012.11.006.

Cota, G., L. Pomeroy, W. Harrison, E. Jones, F. Peters, W. Sheldon Jr., and T. Weingartner (1996), Nutrients, primary production and microbial heterotrophy in the southeastern Chukchi Sea: Arctic summer nutrient depletion and heterotrophy, *Mar. Ecol. Prog. Ser.*, *135*(1), 247–258.

Dosser, H. V., and L. Rainville (2016), Dynamics of the changing near-inertial internal wave field in the Arctic Ocean, *J. Phys. Oceanogr.*, *46*(2), 395–415, doi:10.1175/jpo-d-15-0056.1.

Fer, I. (2006), Scaling turbulent dissipation in an Arctic fjord, *Deep Sea Res., Part II.*, *53*, 77–95, doi:10.1016/j.dsr2.2006.01.003, IAPSO/SCOR Conference on Ocean Mixing.

Fer, I. (2009), Weak vertical diffusion allows maintenance of Cold Halocline in the Central Arctic, *Atmos. Oceanic Sci. Lett.*, *2*(3), 148–152, doi:10.1080/16742834.2009.11446789.

Garrett, C., and W. Munk (1975), Space-time scales of internal waves: A progress report, *J. Geophys. Res.*, *80*(3), 291–297, doi:10.1029/JC080i003p00291.

Gosselin, M., M. Levasseur, P. A. Wheeler, R. A. Horner, and B. C. Booth (1997), New measurements of phytoplankton and ice algal production in the Arctic Ocean, *Deep Sea Res., Part II*, *44*(8), 1623–1644, doi:10.1016/S0967-0645(97)00054-4.

Granskog, M., P. Assmy, S. Gerland, G. Spreen, H. Steen, and L. Smedsrud (2016), Arctic research on thin ice: Consequences of Arctic sea ice loss, *Eos Trans. AGU*, *97*, 22–26, doi:10.1029/2016eo044097.

Guthrie, J. D., J. H. Morison, and I. Fer (2013), Revisiting internal waves and mixing in the Arctic Ocean, *J. Geophys. Res. Oceans*, *118*, 3966–3977, doi:10.1002/jgrc.20294.

Haine, T. W., et al. (2015), Arctic freshwater export: Status, mechanisms, and prospects, *Global Planet. Change*, *125*, 13–35, doi:10.1016/j.gloplacha.2014.11.013.

Honjo, S., R. A. Krishfield, T. I. Eglinton, S. J. Manganini, J. N. Kemp, K. Doherty, J. Hwang, T. K. McKee, and T. Takizawa (2010), Biological pump processes in the cryopelagic and hemipelagic Arctic Ocean: Canada Basin and Chukchi Rise, *Prog. Oceanogr.*, *85*(34), 137–170, doi:10.1016/j.pocean.2010.02.009.

Iversen, T., et al. (2013), The Norwegian Earth system model, NorESM1-M—Part 2: Climate response and scenario projections, *Geosci. Model Dev.*, *6*(2), 389–415, doi:10.5194/gmd-6-389-2013.

Kunze, E., E. Firing, J. M. Hummon, T. K. Chereskin, and A. M. Thurnherr (2006), Global Abyssal mixing inferred from lowered ADCP Shear and CTD strain profiles, *J. Phys. Oceanogr.*, *36*(8), 1553–1576, doi:10.1175/JPO2926.1.

Lique, C., J. D. Guthrie, M. Steele, A. Proshutinsky, J. H. Morison, and R. Krishfield (2014), Diffusive vertical heat flux in the Canada Basin of the Arctic Ocean inferred from moored instruments, *J. Geophys. Res. Oceans*, *119*, 496–508, doi:10.1002/2013JC009346.

McPhee, M. G., G. A. Maykut, and J. H. Morison (1987), Dynamics and thermodynamics of the ice/upper ocean system in the marginal ice zone of the Greenland Sea, *J. Geophys. Res.*, *92*(C7), 7017–7031, doi:10.1029/JC092iC07p07017.

McPhee, M. G., T. P. Stanton, J. H. Morison, and D. G. Martinson (1998), Freshening of the upper ocean in the Arctic: Is perennial sea ice disappearing?, *Geophys. Res. Lett.*, *25*(10), 1729–1732, doi:10.1029/98GL00933.

Morison, J., R. Kwok, C. Peralta-Ferriz, M. Alkire, I. Rigor, R. Andersen, and M. Steele (2012), Changing Arctic Ocean freshwater pathways, *Nature*, *481*(7379), 66–70, doi:10.1038/nature10705.

Morison, J. H., C. E. Long, and M. D. Levine (1985), Internal wave dissipation under sea ice, *J. Geophys. Res.*, *90*(C6), 11,959–11,966.

Nummelin, A., M. Ilicak, C. Li, and L. H. Smedsrud (2015), Consequences of future increased Arctic runoff on Arctic Ocean stratification, circulation, and sea ice cover, *J. Geophys. Res. Oceans*, *121*, 617–637, doi:10.1002/2015jc011156.

Olli, K., et al. (2007), The fate of production in the central Arctic Ocean—Top-down regulation by zooplankton expatriates?, *Prog. Oceanogr.*, *72*(1), 84–113, doi:10.1016/j.pocean.2006.08.002.

Osborn, T. R. (1980), Estimates of the local rate of vertical diffusion from dissipation measurements, *J. Phys. Oceanogr.*, *10*(1), 83–89, doi:10.1175/1520-0485(1980)010<0083:EOTLRO>2.0.CO;2.

Pomeroy, L. R. (1997), Primary production in the Arctic Ocean estimated from dissolved oxygen, *J. Mar. Syst.*, *10*(14), 1–8, doi:10.1016/S0924-7963(96)00059-0.

Randelhoff, A., A. Sundfjord, and A. H. H. Renner (2014), Effects of a shallow pycnocline and surface meltwater on sea ice-ocean drag and turbulent heat flux, *J. Phys. Oceanogr.*, *44*(8), 2176–2190, doi:10.1175/jpo-d-13-0231.1.

Randelhoff, A., A. Sundfjord, and M. Reigstad (2015), Seasonal variability and fluxes of nitrate in the surface waters over the Arctic shelf slope, *Geophys. Res. Lett.*, *42*, 3442–3449, doi:10.1002/2015GL063655.

Randelhoff, A., I. Fer, A. Sundfjord, J.-E. Tremblay, and M. Reigstad (2016), Vertical fluxes of nitrate in the seasonal nitracline of the Atlantic sector of the Arctic Ocean, *J. Geophys. Res. Oceans*, *121*, doi:10.1002/2016JC011779, in press.

Sakamoto, C. M., K. S. Johnson, and L. J. Coletti (2009), Improved algorithm for the computation of nitrate concentrations in seawater using an in situ ultraviolet spectrophotometer, *Limnol. Oceanogr. Methods*, *7*, 132–143.

Sirevaag, A., and I. Fer (2012), Vertical heat transfer in the Arctic Ocean: The role of double-diffusive mixing, *J. Geophys. Res.*, *117*, C07010, doi:10.1029/2012JC007910.

Timmermans, M.-L., J. Toole, R. Krishfield, and P. Winsor (2008), Ice-tethered profiler observations of the double-diffusive staircase in the Canada basin thermocline, *J. Geophys. Res.*, *113*, C00A02, doi:10.1029/2008JC004829.

Timmermans, M.-L., A. Proshutinsky, R. A. Krishfield, D. K. Perovich, J. A. Richter-Menge, T. P. Stanton, and J. M. Toole (2011), Surface freshening in the Arctic Ocean's Eurasian Basin: An apparent consequence of recent change in the wind-driven circulation, *J. Geophys. Res.*, *116*, C00D03, doi:10.1029/2011JC006975.

Torres-Valdés, S., T. Tsubouchi, S. Bacon, A. C. Naveira-Garabato, R. Sanders, F. A. McLaughlin, B. Petrie, G. Kattner, K. Azetsu-Scott, and T. E. Whitledge (2013), Export of nutrients from the Arctic Ocean, *J. Geophys. Res. Oceans*, *118*, 1625–1644, doi:10.1002/jgrc.20063.

Tremblay, J.-E., L. G. Anderson, P. Matrai, P. Coupel, S. Bélanger, C. Michel, and M. Reigstad (2015), Global and regional drivers of nutrient supply, primary production and CO_2 drawdown in the changing Arctic Ocean, *Prog. Oceanogr.*, *139*, 171–196, doi:10.1016/j.pocean.2015.08.009.

Ulfsbo, A., N. Cassar, M. Korhonen, S. van Heuven, M. Hoppema, G. Kattner, and L. G. Anderson (2014), Late summer net community production in the central Arctic Ocean using multiple approaches, *Global Biogeochem. Cycles*, *28*, 1129–1148, doi:10.1002/2014GB004833.

Wassmann, P., et al. (2004), Particulate organic carbon flux to the Arctic Ocean sea floor, in *The Organic Carbon Cycle in the Arctic Ocean*, edited by R. Stein and R. W. Macdonald, pp. 101–138, Springer, Berlin, doi:10.1007/978-3-642-18912-8.

Yamazaki, H., and T. Osborn (1990), Dissipation estimates for stratified turbulence, *J. Geophys. Res.*, *95*(C6), 9739–9744, doi:10.1029/JC095iC06p09739.

Zheng, Y., P. Schlosser, J. H. Swift, and E. Jones (1997), Oxygen utilization rates in the Nansen Basin, Arctic Ocean: Implications for new production, *Deep Sea Res., Part I*, *44*(12), 1923–1943, doi:10.1016/S0967-0637(97)00046-0.